SUPPLEMENTAL TEXT AND FIGURES

Formation of Mixed-layer Sulfide-hydroxide Minerals from the Tochilinite-Valleriite Group During Experimental Serpentinization of Olivine

Thomas M. McCollom[1], Tori Hoehler[2], David A. Fike[3], Jennifer L. Houghton[3], Aaron Bell[4], Frieder Klein[5], Bruce Moskowitz[6], and Peter Solheid[6]

[1]Laboratory for Atmospheric and Space Physics and [4]Department of Geological Sciences, University of Colorado, Boulder CO 80309, USA; [2]NASA Ames Research Center, Moffett Field, CA 94035 USA; [3]Department of Earth and Planetary Sciences, Washington University in St. Louis, St. Louis, M0 63130; [5]Department of Marine Chemistry and Geochemistry, Woods Hole Oceanographic Institution, Woods Hole, MA 02543; [6]Department of Earth and Environmental Sciences and Institute for Rock Magnetism, University of Minnesota, Minneapolis, MN 55455

Contents:

S1. Detailed Analytical Methods
Supplemental Figures S1-S9

S1. Detailed Analytical Methods

Analyses of dissolved H_2, total dissolved CO_2, CH_4, and C_2-C_6 hydrocarbons were performed using procedures described in detail in McCollom et al. (2001) and McCollom and Seewald (2001). Briefly, concentrations of total dissolved CO_2 ($\Sigma CO_2 = CO_{2(aq)} + HCO_3^- + CO_3^{2-}$) were determined by gas chromatography (GC) with thermoconductivity detection (TCD) following acidification of the sample with 25% phosphoric acid and extraction into a headspace with 1 ml He gas. Measured amounts of ΣCO_2 were corrected to account for the fraction remaining dissolved in the acidified fluid. Methane and hydrocarbons were analyzed on the same sample using Flame Ionization Detection (FID). Dissolved H_2 was analyzed on separate samples using a GC with thermoconductivity detection (TCD) following a headspace extraction with 1 ml N_2.

The $pH_{25°C}$ was measured using a Ross micro combination electrode at room temperature with an uncertainty of approximately ±0.1 units of the reported value. Dissolved SiO_2 was measured immediately after sampling with a Hach DR/2400 spectrophotometer using the heteropoly-blue method at a wavelength of 815 nm, with reagents and methods supplied by the manufacturer. An aliquot of the fluid was retained for analysis of major elements after dilution and acidification with a small amount of HNO_3, and subsequently analyzed for total dissolved Na, Ca, Mg, Fe, K, Al, and S by Inductively Coupled Plasma – Optical Emission Spectroscopy (ICP-OES) by Activation Laboratories (Ancaster, Ontario, Canada). Dissolved chloride was analyzed by ion chromatography using standard methods.

To determine concentrations of dissolved sulfate and sulfide, an aliquot of fluid obtained using a gas-tight syringe was injected into an evacuated glass vial containing Zn-acetate in order to precipitate Zn-sulfide for quantification of total dissolved H_2S ($\Sigma H_2S = H_2S_{(aq)} + HS^-$). After vigorously shaking the vial to disperse the fine ZnS particles, a small aliquot (approx. 0.2 ml) was taken and diluted 5× for measurement of total dissolved sulfide. Sulfide determination was done using the Cline method (Cline, 1969), where a 1 ml aliquot of the (filtered and diluted) sample was taken and immediately fixed in cline reagent and allowed to react for 2 hours. The absorbance at 664nm wavelength was measured on a UV-Vis spectrometer (Thermo Evolution 60) along with a set of standards used to calculate sulfide concentration. To determine aqueous sulfate abundance, an additional small aliquot (approx. 0.2 ml) of the fluid sample was then taken from the vial and diluted 15× for total sulfate (ΣSO_4) measurement on a Metrohm Compact IC Pro along with a set of standards used to calculate sulfate concentration. The sulfate samples were run through a 0.2 µm filter before analysis in order to remove any ZnS precipitate.

The sulfur isotopic compositions of dissolved sulfate and solid materials were analyzed using a Thermo Delta C Plus isotope-ratio mass spectrometer (IRMS) at Washington University in St. Louis. The isotopic composition of dissolved sulfate was performed by addition of barium chloride to a fluid aliquot followed by combustion of the resulting barium sulfate, using a set of calibration standards prepared by diluting the initial [34]S-labeled artificial seawater solution with natural abundance sulfate. The olivine and FeS used as reactants were combusted with a Costech ECS 4010 Elemental Analyzer and the products measured using thermal conductivity for sulfur abundance and using IRMS for sulfur isotopic composition. After completion of the experiments, remaining sulfate minerals were removed from the solid products and the chromium-reducible sulfur (CRS) component of the solids was extracted and purified as silver sulfide following methods described in Houghton et al. (2022). The isotopic composition of the silver sulfide yield was analyzed by IRMS using the same calibration methods as the [34]S-labeled barium sulfate precipitates.

Sulfur isotope compositions are expressed in standard delta notation as permil (‰) deviations from the Vienna Canyon Diablo Troilite (VCDT) standard. Natural abundance samples (e.g., initial olivine and pyrrhotite minerals) were calibrated using 3 in-house standards that have been calibrated against international standards IAEA-S-1 (−0.3‰; Robinson, 1995), IAEA-S-3 (−32.5‰; Mann et al., 2009), and NBS-127 (+21.1‰; Coplen et al., 2002). Measurement uncertainty was monitored throughout the analyses using check standards with well-characterized isotopic compositions: Ag_2S (0.3‰ ± 0.35), $BaSO_4$ (+14.5‰ ± 0.33), and ZnS (−5.5‰ ± 0.55).

Initial characterization of the morphology and chemical composition of solid reaction products was performed using a Hitachi SU3500 Scanning Electron Microscope (SEM) equipped with an Oxford Instruments Electron-dispersive X-Ray Spectrometer (EDS) and AZTEC data processing software. Solids for SEM/EDS were examined both as grains mounted on Al stubs with carbon tape and as polished thin sections embedded in epoxy and coated with carbon, using an accelerating voltage of 15 kV. Analysis of the products by X-Ray diffraction (XRD) was performed using a Terra instrument (Olympus, Inc.) with Cu Kα radiation.

Compositional analyses by EMPA and WDS scans measuring the sulfur Kα wavelength shifts were acquired on a JEOL 8230 electron microprobe housed in the Department of Geological Sciences at the University of Colorado Boulder. All measurements were made using a beam energy of 15 keV, a beam current was 10 nA, and a 1 micrometer beam diameter. Both unknown and standard peak intensities were corrected for deadtime, and a ZAF matrix correction algorithm was applied to the raw intensities using mass absorption coefficients FFAST database (NIST v 2.1, 2005). Sulfur Kα WDS scans were performed at using a large area PET crystal using a ~0.15 eV step-width interval and one second dwell time per point. Owing to the small grain sizes and low abundance of reaction products, EMPA analyses were limited to a relatively small number of points in individual experiments. In addition, the small grain size and high porosity of the secondary products resulted in low wt% totals for many of the analyses, so measured compositions have relatively high uncertainties. However, the exact uncertainties are difficult to quantify.

Raman spectra of chrysotile and brucite were obtained at Woods Hole Oceanographic Institution using a Horiba LabRAM HR confocal spectrometer equipped with a 17 mW 633 nm HeNe laser, an astigmatic flat field spectrograph with a focal length of 800 mm, and a multichannel air-cooled (-70 °C) CCD detector. Individual spectra were recorded using a 40× long-distance objective. A grating with 600 grooves / mm and a confocal hole diameter of 100 to 200 μm was chosen for most analyses. Spectra were collected for 5 seconds with 3 accumulations between 100 cm^{-1} and 1300 cm^{-1} and between 3500 cm^{-1} and 3800 cm^{-1}. Raman spectra for haapalaite and valleriite were collected using a Horiba LabRAM HR Evolution Raman spectrometer at the Raman Microspectroscopy Laboratory, University of Colorado-Boulder. The 532 nm laser beam was passed through a polarization scrambler and focused through a 50x or 100x objective lens. A 600 lines/mm diffraction grating and 100 μm confocal pinhole size were used. The spectrometer was calibrated using the 520 cm^{-1} Raman peak of Si prior to analysis.

Mössbauer spectroscopy and magnetic investigations were carried out on powdered samples (~100 mg) at the Institute for Rock Magnetism (IRM), University of Minnesota, USA. Mössbauer spectra were measured at room temperature using a conventional constant-acceleration spectrometer (model MS6, SeeCo, USA) in transmission geometry with a ^{57}Co/Rh source. An α-Fe foil at room temperature was used to calibrate isomer shifts and velocity scale. Mössbauer spectra were fit by least-squares to sums of Lorentzian lines using custom software to obtain estimates for isomer shift (IS), quadrupole splitting (QS), hyperfine field (B_{HF}), linewidth (Γ), and relative area (A) for each subspectrum. Uncertainties for Mössbauer parameters are ±0.01 mm/s

for IS and QS, and ±5% for spectral area. To focus on secondary products (primarily Fe in serpentine), samples for Mössbauer analysis were physically separated from the bulk solids by sonication with ethanol in a glass vial followed by removal of the suspended fraction. This procedure was repeated until the ethanol was no longer cloudy, and Mössbauer analysis performed on this prepared sample following evaporation of the ethanol. Magnetite was removed from products during this process using a strong magnet placed next to the vial. Analysis of the treated solids with XRD indicated that this process was successful in increasing the proportion of chrysotile and other secondary products, but a substantial amount of unreacted olivine still remained owing to its small grain size (Fig. S3).

Samples for magnetic analysis were prepared by packing approximately 200 mg of bulk reacted solids into #4 gelatin capsules and then placing them in plastic straw holders. Room temperature hysteresis loops were obtained in a vibrating sample magnetometer (Model 3900, Princeton Corporation Measurements) using an electromagnet to produce fields up to 1 T. Hysteresis parameters (saturation magnetization, M_s; saturation remanence, M_r; coercivity, B_c) were calculated after paramagnetic slope correction over the interval of 0.7-1.0 T using the non-linear approach-to-saturation fitting method of Jackson and Solheid (2010). The magnetite weight-percent was determined from the room-temperature bulk saturation magnetization values and the known value for pure magnetite (M_s=92 Am^2/kg) as follows:

$$\text{Magnetite weight percent} = \frac{M_s(sample)}{M_s(magnetite)} \times 100 \text{ percent.}$$

Magnetic measurements at low-temperatures (20-300 K) were used to identify characteristic magnetic transitions for magnetite (Verwey transition at ~120 K) and pyrrhotite (Besnus transition at ~34 K). Low temperature remanent magnetization curves were obtained with a SQUID magnetometer (Quantum Design, San Diego, CA, USA – MPMS-XL). The data were obtained by cooling the sample to 10 K in a 2.5 T field (Field cooled (FC) magnetization). The field was then reduced to zero and the remanent magnetization was measured on warming to 300 K in 5 K steps.

Thermogravimetric analyses (TGA) were performed at Woods Hole Oceanographic Institution on the reacted solids to determine the amount of hydrated minerals present, and these data were then used to estimate the amount of primary minerals reacted. The analyses were performed using a Thermal Analysis (TA) Instruments (Lindon, UT) SDT Q600 simultaneous thermogravimetric analyzer-differential scanning calorimeter. Finely ground samples (~30-50 mg) were weighed into an alumina crucible and heated from room temperature to 1100 °C at 10 °C per minute while monitoring the change in mass and heat flow. An empty crucible was measured as a blank value simultaneous with the sample to minimize errors in sample weighing during heating. Nitrogen (N_2) was used as the purge gas at a flow rate of 50 ml per minute. Weight loss between 320°C and 420°C was assigned to brucite, while that between 450°C and 700°C was assigned to serpentine (Viti, 2010; Klein et al., 2020).
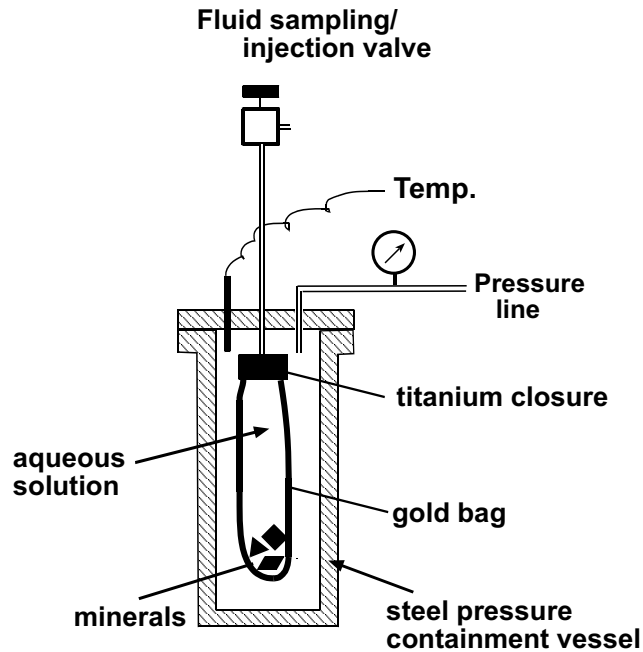
Additional References Cited in Supplemental Text

Blaauw, C., Stroink, G., Leiper, W., and Zentilli, M. (1979) Crystal-field properties of Fe in brucite $Mg(OH)_2$. Physica Status Solidi B **92**, 639-643.

Coplen, T. B., Hopple, J. A., Böhlke, J. K., Peiser, H. S., Rieder, S. E., Krouse, H. R., Rosman, K. J. R., Ding, T., Vocke, R. D. J., Révész, K. M., Lamberty, A., Taylor, P., and DeBièvre, P. (2002) Compilation of Minimum and Maxium Isotope Ratios of Selected Elements in Naturally Occurring Terrestrial Materials and Reagents, United States Geological Survey, pp. 98.

Gubaidulina, T. V., Chistyakova, N. I., and Rusakov, V. S. (2007) Mössbauer study of layered iron hydroxides: Tochilinite and Valleriite. Bulletin of the Russian Academy of Science, **71**, 1269-1272.

Houghton, J., Scarponi, D., Carparo, L., and Fike, D. A. (2022) Impact of sedimentation, climate and sea level on marine sedimentary pyrite sulfur isotopes: Insights from the Valle di Manche section (Lower-Middle Pleistocene, southern Italy). Palaeogeography, Palaeoclimatology, Palaeoecology, **585**, 110730

Jackson, M., and Solheid, P. (2010), On the quantitative analysis and evaluation of magnetic hysteresis data. Geochemistry Geophysics Geosystems, 11, Q04Z15, doi: 10.1029/2009GC002932.

Mann, J.L., Vocke, R.D., Jr., and Kelly, W.R. (2009) Revised $\delta^{34}S$ Reference Values for IAEA Sulfur Isotope Reference Materials S-2 and S-3. Rapid Communications in Mass Spectrometry, **23**, 1116–1124.

McCollom, T. M., and Seewald, J. S. (2001) A reassessment of the potential for reduction of dissolved CO_2 to hydrocarbons during serpentinization of olivine. Geochimica et Cosmochimica Acta **65**, 3769-3778.

McCollom, T. M., Seewald, J. S., and Simoneit, B. R. T. (2001) Reactivity of monocyclic aromatic compounds under hydrothermal conditions. Geochimica et Cosmochimica Acta, **65**, 455-468.

McCollom, T. M., Klein, F., Robbins, M., Moskowitz, B., Berquó, T. S., Jöns, N., Bach, W., and Templeton, A. (2016) Temperature trends for reaction rates, hydrogen generation, and partitioning of iron during experimental serpentinization of olivine. Geochimica et Cosmochimica Acta, **181**, 175-200.

O'Hanley, D. S., and Dyar, M. D. (1993) The composition of lizardite 1T and the formation of magnetites in serpentinites. American Mineralogist, **78**, 391-404.

O'Hanley, D. S., and Dyar, M. D. (1998) The composition of chrysotile and its relationship with lizardite. Canadian Mineralogist **36**, 727-739.

Robinson, B.W. (1995) Sulphur isotope standards. Reference and intercomparison materials for stable isotopes of light elements. International Atomic Energy Agency, Vienna, Austria. IAEA-TECDOC-825, 39-45.

Viti, C. (2010) Serpentine minerals discrimination by thermal analysis. American Mineralogist, **95,** 631-638.
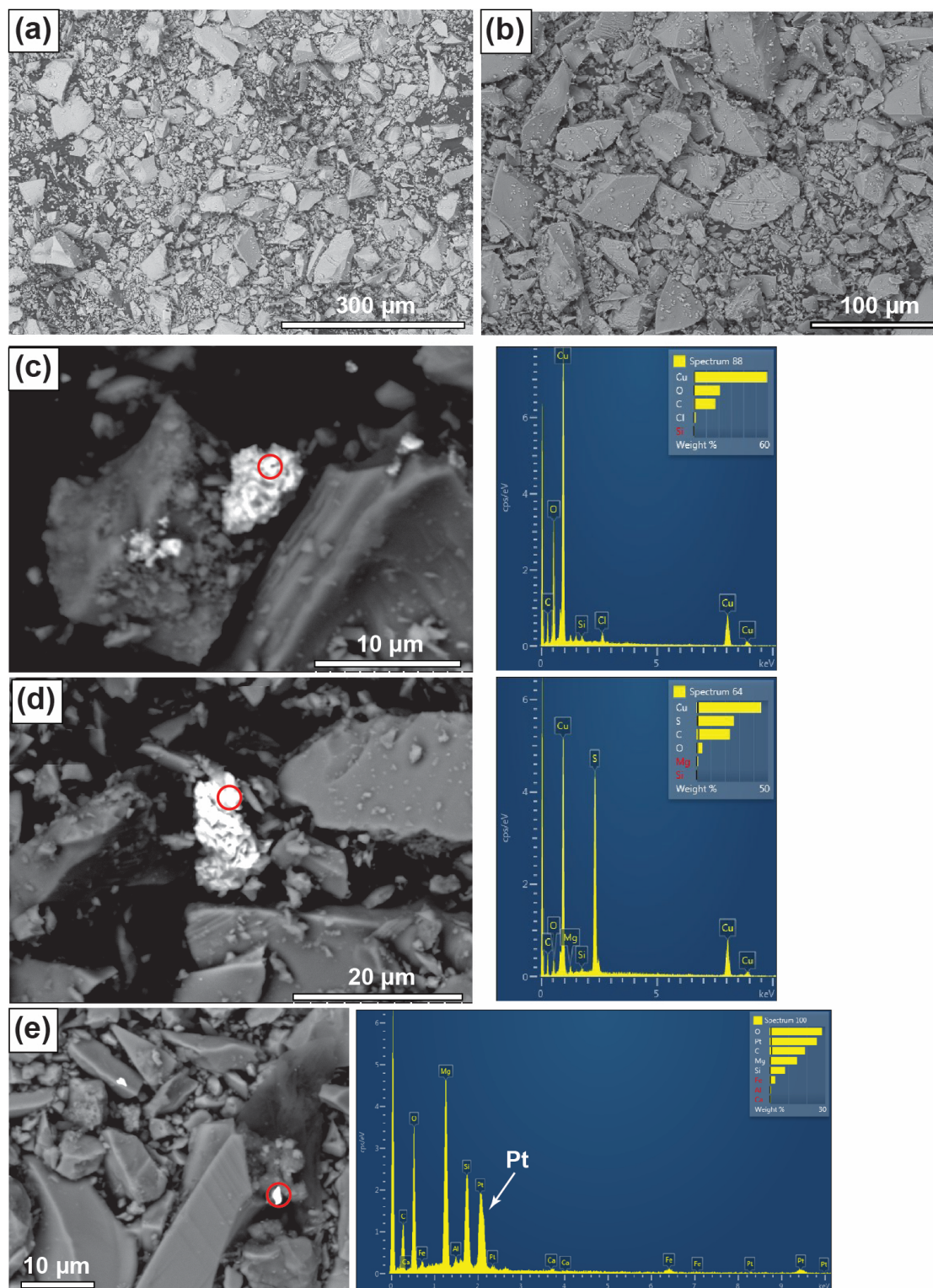
Supplemental Table S1. Compositions of TVG minerals from experiments compared with several examples from natural samples, with all compositions normalized to the format commonly adopted for TVG minerals (e.g., Beard, 2000).

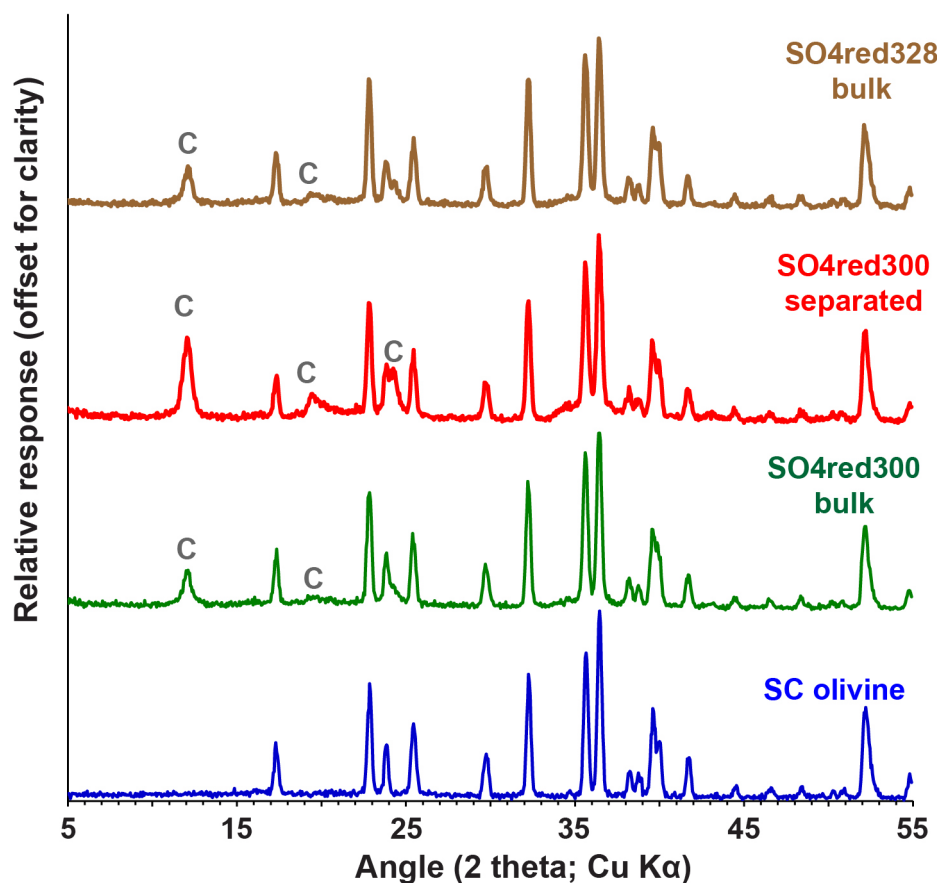| Sample	SO4red328 Valleriite	SO4red300 Haapalaite	Hole 1068A Tochilinite	Hole 1068A "Cu rich"	Hole 1068A "Ni rich"	Hole 1068A "Ni rich"	Kaveltorp Valleriite	Kaveltorp Valleriite	Loolekop Valleriite	Del Norte, CA Vallerite	Outokumpu Haapalaite[*]
S	19.1	18.4	21.3	17.5	20.0	20.1	22.3	21.4	20.6		22.0
Fe	20.1	18.9	34.7	17.8	25.5	27.1	21.5	21.2	19.8[y]		24.1
Cu	11.7	0.0	0.0	13.0	0.00	0.00	18.7	17.6	21.6		0.1
Ni	4.0	14.6	2.2	1.2	9.7	8.4					14.9
Co	0.0	0.1	0.3	0.0	0.02	0.0					0.0
MgO	16.6	18.1	17.8	16.1	16.5	17.5	17.9	16.2	16.0		18.8
FeO	2.5	5.0	4.0	22.2	6.1	3.6					6.4
SiO2	1.8	0.62	0.68	0.0	0.15	0.34	1.75				-
Al2O3	2.7	1.19	1.32	2.3	4.6	5.1	6.09	8.1	8.5		0.2
CaO							0.93	1.7	1.3		
Total	78.6	81.3	82.2	90.2	82.6	82.1	89.2	86.2	87.8		86.5
Sulfide layer (mole fraction)											
Fe	0.59	0.58	0.94	0.59	0.74	0.78	0.57	0.58	0.47	0.67	0.63
Cu	0.30	0.00	0.00	0.38	0.00	0.00	0.43	0.42	0.53	0.33	0.00
Ni	0.11	0.42	0.06	0.04	0.26	0.22					0.37
Co	0.0	0.0	0.01	0.00	0.00	0.00					0.00
Hydroxide layer (mole fraction)											
Mg	0.81	0.78	0.70	0.53	0.70	0.74	0.77	0.69	0.64	0.68	0.83
Fe	0.08	0.16	0.26	0.41	0.15	0.09	0.0	0	0.08	0.18	0.16
Al	0.12	0.06	0.04	0.06	0.16	0.17	0.23	0.31	0.27	0.16	0.01
Sulfide: hydroxide	1.3	1.34	1.04	0.72	1.07	1.09	1.34	1.29	1.04	1.34	1.23
Reference	This study	This study	1	1	1	1	2	2	2	3	4

Data sources: (1) Beard, 2000, (2) Evans and Allmann (1968), (3) Harris et al. (1972), (4) Huhma et al. (1973). [*]Type locality. Note: the cation distributions for the hydroxide layers given in Table T1 of Beard (2000) are inconsistent with the chemical compositions listed in the same table; consequently, the values listed in that publication differ from those provided here
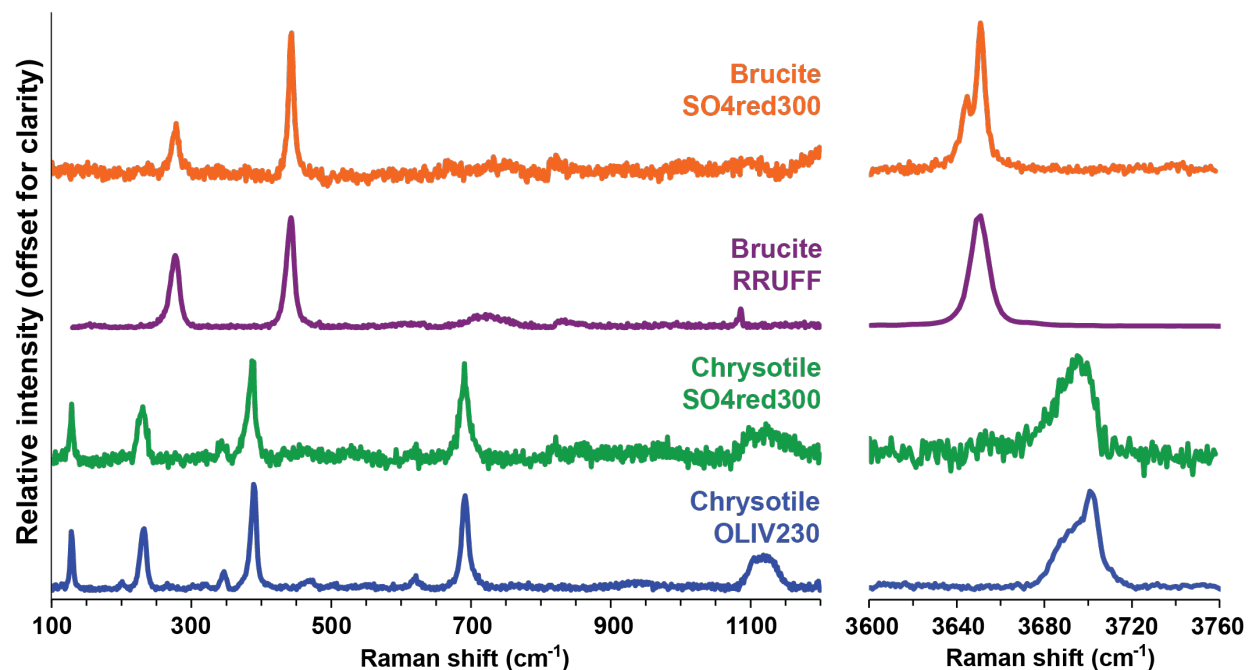
Supplemental Figure S1. Schematic drawing of flexible-cell hydrothermal reaction system used in the experiment SO4red300. The reactor lies horizontal in the furnace during operation.
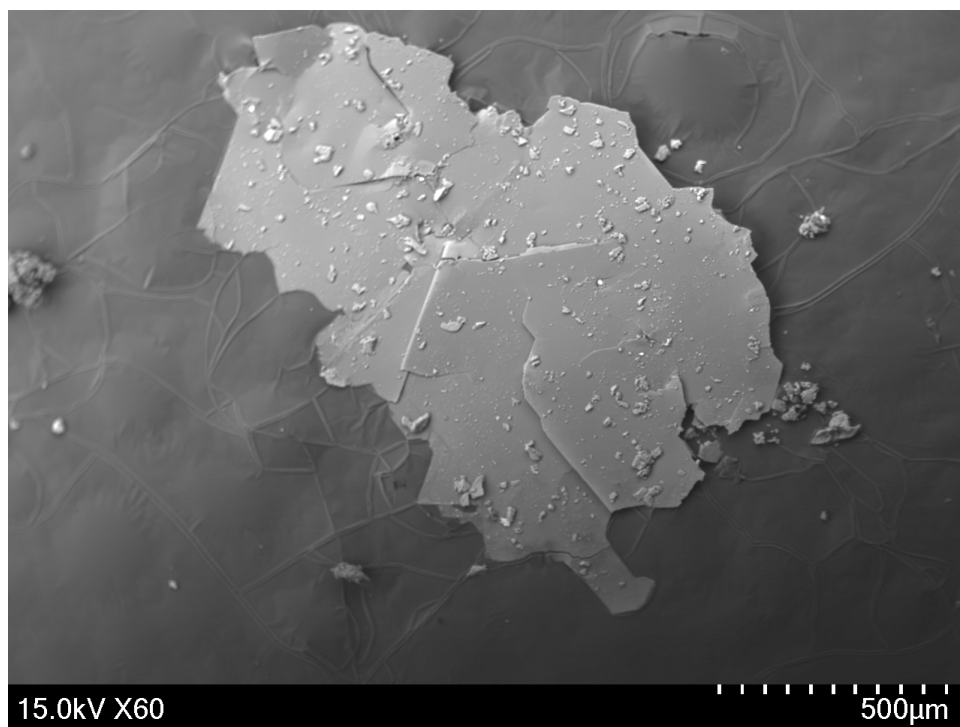
Supplemental Figure S2. Back-scattered electron images of starting materials for experiment SO4red328. (a,b) Overviews of powdered olivine used in experiments. (c) Examples of Cu-oxide particles found sparsely scattered in the powdered olivine. (d) Single Cu-sulfide particle identified in olivine powder. (d) Pair of rare Pt-rich particles. Red circles indicate location of EDS analyses, shown in blue boxes.

Supplemental Figure S3. X-ray diffraction patterns for reactant olivine and for experimental products. For SO4red300, results are shown for both the bulk reacted solids and for materials obtained following treatment to remove some of the residual olivine from the bulk reaction products (see supplemental text for description of separation procedure). All discernible peaks in the reaction products can be attributed to either residual olivine or to chrysotile (C). Analyses performed with Cu Kα radiation.
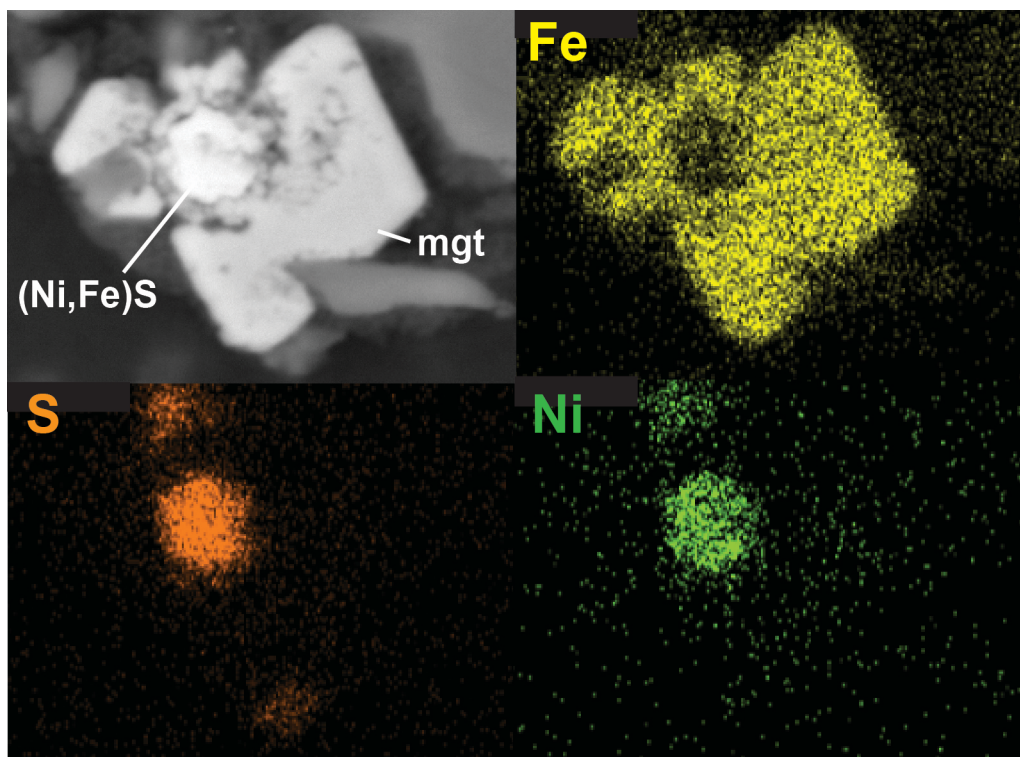
Supplemental Figure S4. Raman spectroscopy analyses of chrysotile and brucite from SO4red300. A spectrum from chrysotile produced during serpentinization of olivine at 230°C is shown for comparison (from McCollom et al., 2016).
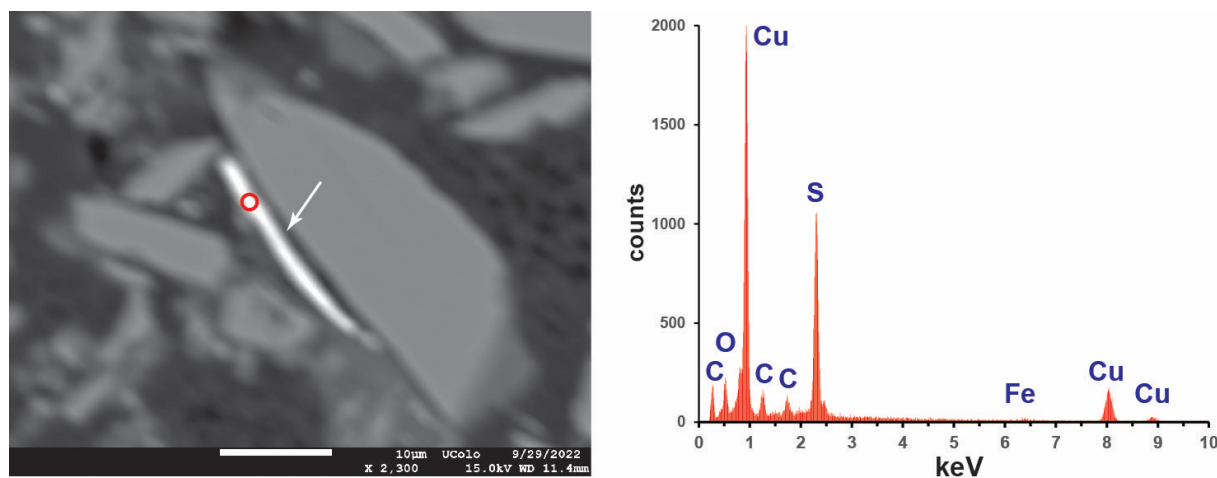
Supplemental Figure S5. Back-scattered electron image of a large brucite crystal picked from the reacted solids from experiment SO4red300 mounted on carbon tape.
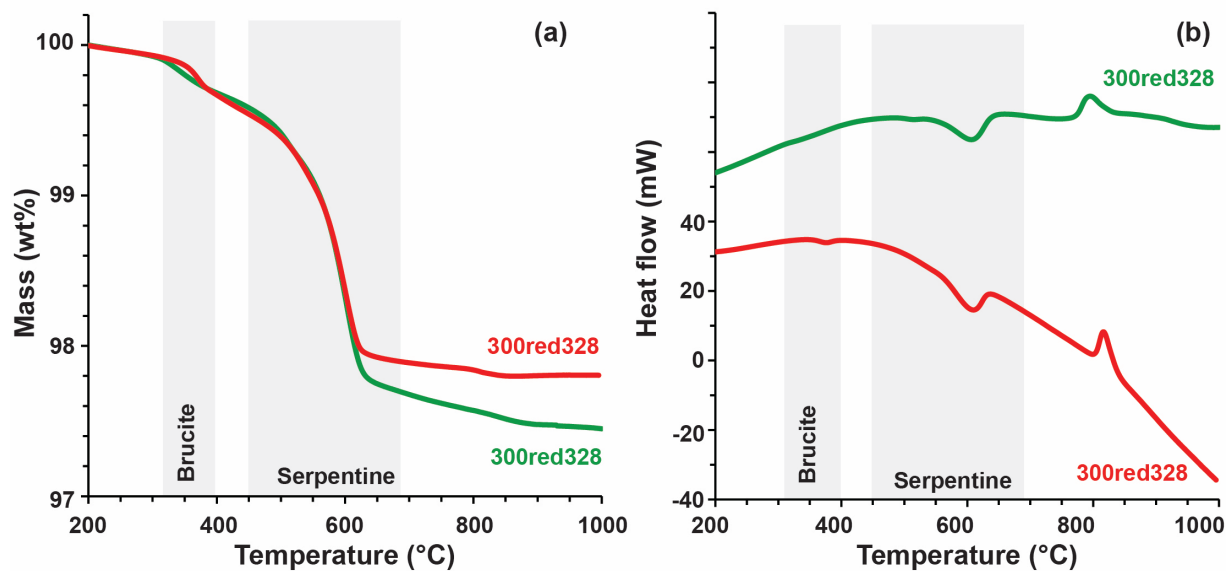
Supplemental Figure S6. Representative back-scattered electron images of a Ca- and S-enriched minerals found sparsely dispersed among the reacted solids of SO4red300. Based on the prismatic shape, chemical composition, and elevated reaction temperature, this mineral is probably anhydrite. (a) Grains mounted on carbon tape. (b) Polished thin section of reacted solids.
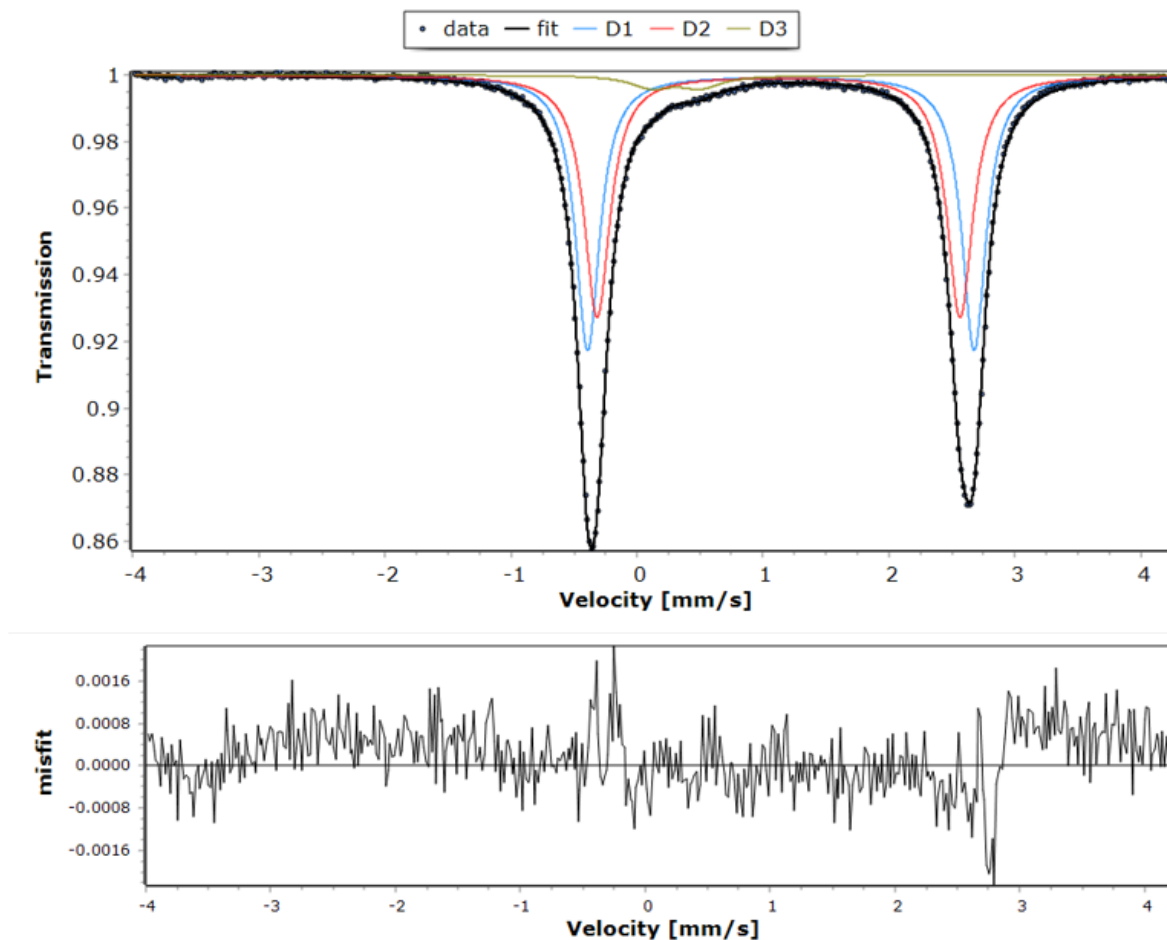
Supplemental Figure S7. Elemental map of (Ni,Fe)-sulfide mineral surrounded by magnetite shown in Figure 4f. From experiment SO4red328.
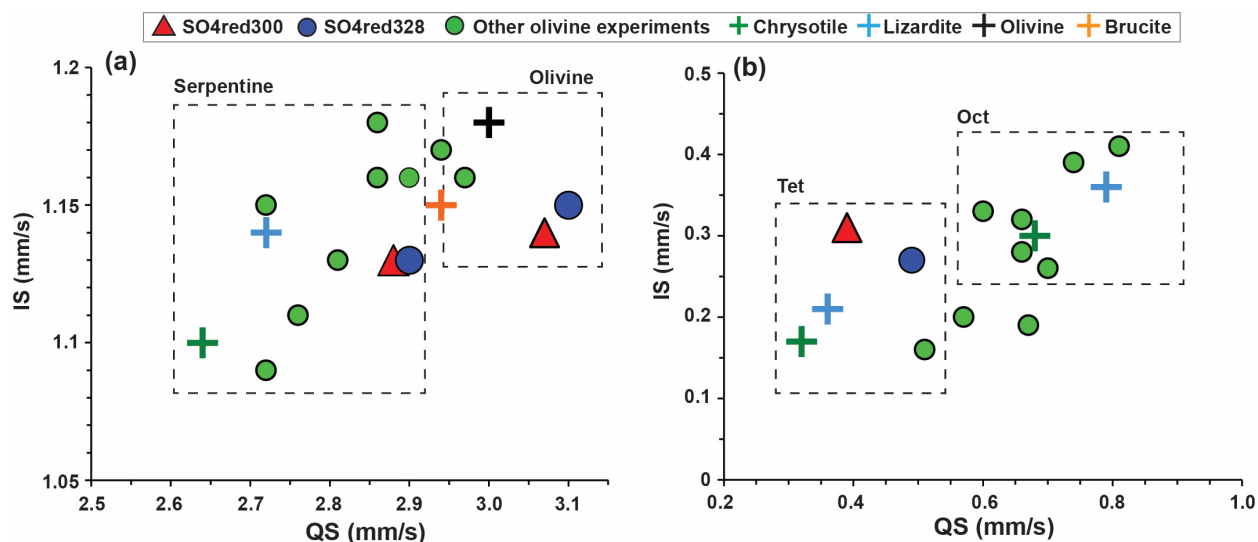
Supplemental Figure S8. Back-scattered electron image of a Cu-sulfide mineral (arrow) from SO4red328. Red circle in image indicates location of EDS analysis shown on right. The EDS results indicate the mineral has a Cu:S ratio of approximately one.

Supplemental Figure S9. Results of thermogravimetric analysis of reacted solids from experiments SO4red300 and SO4red328, including (a) weight loss and (b) heat flow. Mass loss between 320°C and 400°C is assigned to brucite while that occurring between 450°C and 680°C is assigned to serpentine (Viti, 2010).

Supplemental Figure S10. Results of Mössbauer analysis of reacted solids from SO4red300. Prior to analysis, the bulk solids were processed to remove magnetite and some of the unreacted olivine (see text above).

Supplemental Figure S11. Room-temperature hyperfine magnetic Mössbauer parameters for the treated samples from SO4red300 and SO4red328. Also shown for comparison are MB parameters derived for several reference minerals and for chrysotile in other olivine serpentinization experiments (McCollom et al., 2016, and unpublished data). Data for reference minerals are from O'Hanley and Dyar (1993, 1998) and Blaauw et al. (1979). The parameters associated with Fe^{III} in tetrahedral (Tet) and octahedral (Oct) sites of chrysotile are identified in (b).